PCCP

PAPER

View Article Online
View Journal | View Issue

Cite this: *Phys. Chem. Chem. Phys.*, 2017, **19**, 9606

Eu^{2+}–Eu^{3+} valence transition in double, Eu-, and Na-doped PbSe from transport, magnetic, and electronic structure studies

Bartlomiej Wiendlocha,*[ab] SunPhil Kim,[b] Yeseul Lee,[c] Bin He,[b] Gloria Lehr,[d] Mercouri G. Kanatzidis,[c] Donald T. Morelli[d] and Joseph P. Heremans[be]

Received 17th January 2017,
Accepted 20th March 2017

DOI: 10.1039/c7cp00358g

rsc.li/pccp

The Eu atoms in $Pb_{1-x}Eu_xSe$ have long been assumed to be divalent. We show that p-type doping of this magnetic semiconductor alloy with Na can modify the effective Eu valence: a mixed, Eu^{2+}–Eu^{3+} state appears in $Pb_{1-x-y}Eu_xNa_ySe$ at particular values of *y*. Magnetization, carrier concentration, resistivity, and thermopower of $Pb_{1-x-y}Eu_xNa_ySe$ are reported for a number of samples with different *x* and *y*. A pronounced increase in thermopower at a given carrier concentration was identified and attributed to the presence of enhanced ionized impurity scattering. A strong decrease in the hole concentration is observed in $Pb_{1-y}Na_ySe$ when Eu is added to the system, which we attribute to a Eu^{2+}–Eu^{3+} self-ionization process. This is evidenced by magnetization measurements, which reveal a significant reduction of the magnetic moment of $Pb_{1-x}Eu_xSe$ upon alloying with Na. Further, a deviation of magnetization from a purely paramagnetic state, described by a Brillouin function, identifies antiferromagnetic interactions between the nearest-neighbor Eu atoms: a value of $J_{ex}/k_B = -0.35$ K was found for the exchange coupling parameter. The conclusion of a Eu^{2+}–Eu^{3+} self-ionization process being in effect is supported further by the electronic structure calculations, which show that an instability of the $4f^7$ configuration of the Eu^{2+} ion appears with Na doping. Schematically, it was found that the Eu 4f levels form states near enough to the Fermi energy that hole doping can lower the Fermi energy and trigger a reconfiguration of a 4f electronic shell.

Introduction

The Pb-salt semiconductors (PbS, PbSe, and PbTe) have been the earliest practical semiconductors used in electronic devices such as crystal rectifiers, infrared sensors, diode lasers, and thermoelectric generators.[1] Recently, they also have been reported to be potential topological insulators.[2] This class of semiconductors hosts the materials with the highest thermoelectric ZT,[3–5] in particular in alloys in which other divalent elements such as Sr are substituted for Pb^{2+}.[6] PbSe, the binary semiconductor that is the starting point for the present study, is an excellent thermoelectric semiconductor[7,8] that avoids the use of Te, which is not abundant in the earth's crust. Another element thought to be divalent, Eu, is known to increase the band gap of PbTe[9] and PbSe:[10,11] PbEuTe and PbEuSe have been used as the high-gap semiconductor in PbTe and PbSe double-heterojunction, quantum-well, tunable infrared diode lasers.[11] For these applications, the fact that Eu is divalent was one of its main advantages, as compared to other rare earth elements, since it allowed modification the band gap of the material without increasing the carrier concentration.

Magnetic studies have been performed on PbEuTe[12–15] and PbEuSe[9,16,17] alloys and superlattices. The transport properties of PbSe containing various rare-earth elements have been studied more recently.[18] In these works, Eu in PbSe was found to be electrically inactive and magnetic in the Eu^{2+} state, making $Pb_{1-x}Eu_xSe$ one of the dilute magnetic semiconductors (DMS). None of earlier studies include a systematic variation of both the Eu content while adjusting the p-type doping level independently, as is done here with Na-doping. This approach reveals that the valence of Eu is indeed 2+ in material with low carrier concentrations but shifts from 2+ to 3+ upon p-type doping with Na. The second, electrically active impurity (Na^+) controls the valence transition of the 4f shell into the Eu^{3+} state, leading to a mixed $4f^6$–$4f^7$ valence state in the material.

[a] *Faculty of Physics and Applied Computer Science, AGH University of Science and Technology, Aleja A. Mickiewicza 30, 30-059 Krakow, Poland. E-mail: wiendlocha@fis.agh.edu.pl*
[b] *Department of Mechanical & Aerospace Engineering, The Ohio State University, Columbus, Ohio, USA*
[c] *Department of Chemistry, Northwestern University, Evanston, IL, USA*
[d] *Department of Chemical Engineering and Materials Science, Michigan State University, East Lansing, MI, USA*
[e] *Department of Physics, The Ohio State University, Columbus, OH, USA*

This changes both transport and magnetic properties. To the best of our knowledge, this is the first example of a fully controllable and tunable triggering of a valence mixing effect in a dilute magnetic semiconductor by the addition of a second, electrically active element. Moreover, the effect here appears at low doping levels, with charge carrier concentration variations orders of magnitude smaller than, for instance, in metallic $CePd_3$.[19]

Among DMS or metals in which a mixed valence or a valence fluctuation is observed, we mostly find alloys in which the concentration of the transition metal or rare-earth element has been adjusted to release the valence instability. A review of this approach for DMS based on lead chalcogenides is given in ref. 20 and references therein. One of the most studied cases of mixed-valence DMS is Fe-doped HgSe, where iron adopts Fe^{2+} configuration at low doping levels, whereas a mixed Fe^{2+}–Fe^{3+} state appears[21–25] at higher Fe concentration. These two types of iron ions may form an ordered superlattice of Fe^{2+} and Fe^{3+}, leading to unexpectedly high mobility of the carriers[26]. Chromium also was reported to exist in two valence states, as Cr^{2+} and Cr^{3+} in PbTe[27] and PbSe[28]. In all these materials, the transition metal (TM) impurities' valence changed with increasing TM concentration, thus there was no independent way of controlling the valence at any specific composition. Among rare-earth impurities in chalcogenides, Gd and Yb also showed a tendency to change their valence, when the carrier concentration in the samples was varied. However, for the Gd case, the 4f electronic shell configuration remained unchanged: in $Sn_{1-x}Gd_xTe$,[29,30] a transition from Gd^{2+} ($4f^75d^1$) to Gd^{3+} ($4f^75d^0$) was observed and led to modifications of the f–f exchange interactions, but in both cases 4f shell remained half-filled. The Yb behavior in $Pb_{1-x}Ge_xTe$:Yb seems to be more similar to what is reported here for Eu in $Pb_{1-x-y}Na_yEu_xSe$, since the Yb valence change affected the 4f shell configuration, leading to a change in magnetic properties of Yb. It was found[31] that as-grown samples of, *e.g.*, $Pb_{0.985}Ge_{0.01}Yb_{0.005}Te$ were p-type and paramagnetic (*i.e.* Yb was in Yb^{3+} [$4f^{13}$] state), but after annealing transformed to n-type and diamagnetic (*i.e.* Yb was in electrically inactive and nonmagnetic Yb^{2+} [$4f^{14}$] state). However, no valence mixing and no possibility to control the valence was reported in that case, unlike in $Pb_{1-x}Eu_xSe$:Na, reported here. Thus, our findings in $Pb_{1-x}Eu_xSe$:Na offer a new way of inducing and controlling the valence transitions in diluted magnetic semiconductors.

The manuscript is structured further as follows. Samples of $Pb_{1-x-y}Eu_xNa_ySe$ alloys were synthesized using a combined vacuum-melting and spark-plasma sintering (SPS) technique. The transport properties are reported next, and reveal an anomaly in the variation of the charge concentration with increasing Na content y. We show that the Pisarenko relation between the carrier concentration and the thermopower suggests an increase in ionized impurity scattering at a particular value of y, suggesting a sudden change in the valence of Eu from Eu^{2+} to Eu^{3+}. Next, magnetic studies quantitatively confirm this hypothesis. A more detailed study of the deviations of the measured magnetization curves from Brillouin functions reveals the presence of antiferromagnetic interactions between Eu ions. Finally, electronic structure calculations confirm the existence of a density of Eu 4f states near the Fermi energy E_F. By changing the Na doping level one can control the E_F position independently of the Eu concentration and locate it inside the 4f states. The Eu^{2+} configuration in PbSe then can become unstable and mixed Eu^{2+}–Eu^{3+} states appears.

Experimental & theoretical procedure

Elemental Pb (99.99%, American Elements), Se (99.999%, 5N Plus Inc), Na (99.95%, Aldrich), and Eu (99.9%, Chinese Rare Earth Information Center) were used for the synthesis of $Pb_{1-x-y}Eu_xNa_ySe$. Ingots (20 g) with nominal compositions $Pb_{0.99-x}Eu_xNa_{0.01}Se$ (x = 0, 0.01, 0.02, 0.03, 0.04, 0.06, 0.09 and 0.12) and $Pb_{0.99-y}Eu_{0.01}Na_ySe$ (y = 0, 0.01, 0.02, 0.03, and 0.04) were prepared by mixing appropriate ratios of reagents in carbon-coated quartz tubes. The tubes were sealed under vacuum (10^{-4} Torr) and heated to 1423 K over a period of 12 h. The tubes then were soaked at that temperature for 5 h, and rapidly cooled to room temperature over 3 h. The obtained ingots were cleaned and ground to a powder using a mechanical grinder to reduce the particle sizes to less than 53 μm. These powders were densified at 923 K for 5 min under an axial compressive pressure of 40 MPa in an argon atmosphere in an SPS apparatus. Table 1 reports a summary of the samples studied.

Thermoelectric transport properties and galvanomagnetic properties of $Pb_{1-x-y}Eu_xNa_ySe$ samples were measured in a customized cryostat, either with an AC bridge, or with a static heater-and-sink method. The samples were cut into parallelepipeds with dimensions around 2 mm × 2 mm × 10 mm. To minimize heat loss, very thin copper and constantan wires were used as thermocouples. Four-probe measurements were used to measure the resistivity of the samples using 4 copper wires. Hall resistivity was obtained by applying a transverse magnetic field in the range -14 kOe $\leq H \leq +14$ kOe. All the thermoelectric and galvanomagnetic properties were measured in the temperature range 80 K $\leq T \leq$ 420 K. Two experimental measurements of magnetization, M, were conducted using a superconducting quantum interference device (SQUID). The first measurement of M *vs.* temperature was performed by applying a magnetic field of 5 kOe and sweeping the temperature from 2 K to 300 K. From the obtained data, the magnetic susceptibility χ was calculated. The susceptibility of Eu^{2+} was then obtained by subtracting the diamagnetic susceptibility of the PbSe lattice. A second measurement of magnetization was carried out by varying the magnetic field from 0 to 60 kOe at 2 K, 4 K, and 6 K.

Electronic structure calculations were performed using the full potential linearized augmented plane wave (FP-LAPW) method, as implemented in the WIEN2k code.[32] To simulate the doping, the supercell approach was used, building a 64-atom 2 × 2 × 2 supercell, starting from a cubic rock-salt PbSe unit cell (a = 6.12 Å). Spin–orbit interaction was taken into account, and the Coulomb interactions between the 4f Eu

Table 1 Comparison of the obtained Eu^{2+} concentration from magnetization data fitting and estimated based on carrier concentration data at 80 K and 300 K

Samples	Carrier concentration (10^{19} cm^{-3}) 80 K	300 K	Atomic concentration of Eu^{2+} (%) from magnetization fitting (in brackets: percent of the total Eu)	Atomic concentration of Eu^{2+} (%) from carrier concentration (in brackets: percent of the total Eu)
Eu0%:Na 1%	21	17	0	0
Eu1%:Na 1%	6.0	8.2	0.24 (24%)	0.14[a] (14%)
Eu2%:Na 1%	5.2	6.0	1.49 (74%)	1.1[a] (55%)
Eu3%:Na 1%	2.2	3.4	2.03 (68%)	1.92[a] (64%)
Eu6%:Na 1%	2.2	3.6	4.15 (69%)	4.92[a] (82%)
Eu1%:Na 0%	—	0.27	0.93 (93%)	~1 (100%)
Eu1%:Na 2%	—	19	0.15 (15%)	~0 (0%)
Eu1%:Na 3%	—	35	0.06 (6%)	~0 (0%)
Eu1%:Na 4%	—	41	0.017 (1.7%)	~0 (0%)

[a] Calculated based on carrier concentration data at 80 K.

electrons were treated using the LDA + U method. We took U = 7 eV and J = 1 eV, as values of U between 7 eV and 10 eV usually are considered for Eu in the literature.[33,34] The modified Becke–Johnson semilocal exchange potential of Tran and Blaha[35] was used and appeared to be very efficient in its description of the 4f Eu electronic states near the band gap.

Results and discussion

A. Electronic transport properties of $Pb_{1-x-y}Eu_xNa_ySe$

Transport properties (carrier concentration as measured by the Hall effect, thermopower, and resistivity) of $Pb_{1-x-y}Eu_xNa_ySe$, (y = 0.01; x = 0, 0.01, 0.02, 0.03, 0.04, 0.06, 0.12) samples are shown as function of temperature in Fig. 1. The carrier concentrations in the samples (Fig. 1a) reach values between 2 and 22 × 10^{19} cm^{-3}, and exhibit a small temperature dependence, most likely due to the temperature dependence of the Hall prefactor.[36] The hole concentration values at 80 K and 300 K of all samples are summarized in Table 1. We did not obtain a Hall measurement on the lowest-doped sample with the highest Eu content (x = 0.12, y = 0.01), because its resistivity was too high. We also measured a $Pb_{0.99}Eu_{0.01}Se$ sample without any Na doping, not included in Fig. 1, and its Hall effect showed a hole concentration of about 3 × 10^{18} cm^{-3} at room temperature. The thermopower scales appropriately with the carrier concentration, and varies mostly linearly with temperature over the measurement range, except for the lowest-doped samples. The resistivity of most samples is quite high: the presence of Eu in the samples decreases the mobility by factors varying from 2 (x = 0.01) to over an order of magnitude (x = 0.06) when

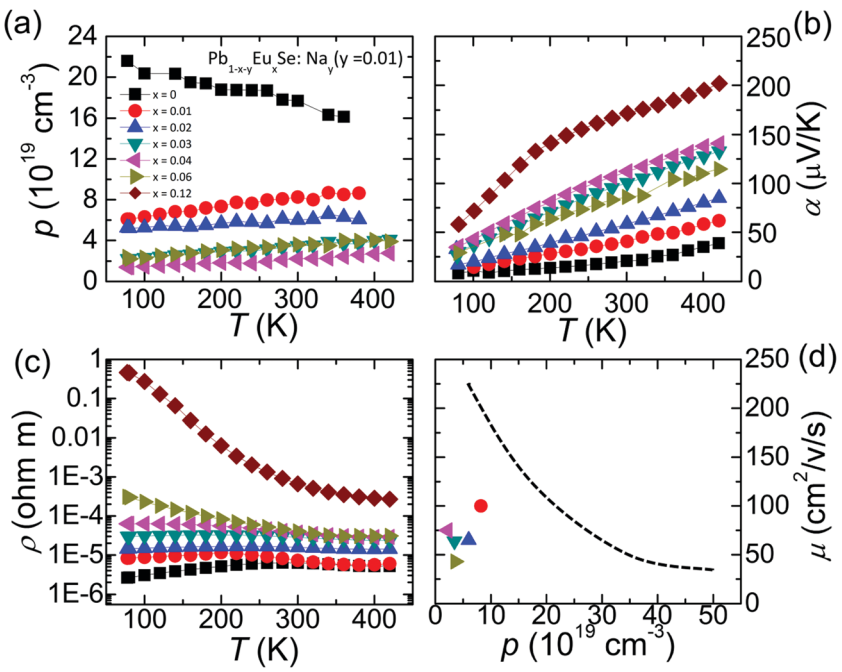

Fig. 1 Temperature-dependent transport properties of $Pb_{1-x-y}Eu_xNa_ySe$ (a) carrier concentration from Hall effect measurements $p(T)$, (b) thermopower $\alpha(T)$, (c) resistivity $\rho(T)$, (d) mobility (μ) comparison at T = 300 K. The black dashed line, taken after ref. 7, represents mobility of Na-doped PbSe with differing Na doping level.

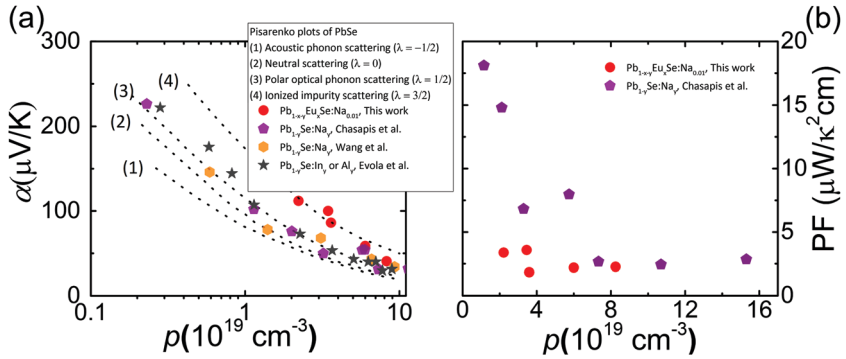

Fig. 2 (a) The Pisarenko plot (thermopower *vs.* carrier concentration) of PbSe with different doping elements, as described in the legend. The dotted lines are theoretical Pisarenko relations computed assuming different scattering exponents[37,39] (see, text). Experimental points are taken from ref. (Evola *et al.*[37]), (Chasapsis *et al.*[40]), (Wang *et al.*[41]); (b) comparison of the room-temperature power factor (PF) for double-doped and Na-doped PbSe.

compared to similarly-doped Eu-free PbSe, as shown in Fig. 1d. The Pisarenko relation (thermopower *versus* the carrier concentration) of PbSe at room temperature of the samples is shown in Fig. 2a where we include data taken from the literature on other PbSe samples. The dashed lines in Fig. 2a are theoretical curves, adopted from ref. 37, and are calculated using the non-parabolic Kane model, literature values of valence band effective masses,[38] and assuming four different dominating scattering mechanisms, represented by appropriate scattering exponents λ (see also ref. 39 for more details). Here, the scattering exponent describes the energy dependence of the hole relaxation time $\tau(E)$, which is assumed to follow a power law $\tau(E) = \tau_0 \frac{\gamma^{\lambda}}{\gamma'}$, where the term $\gamma \equiv \gamma(E) = E\left(1 + \frac{E}{E_g}\right)$, instead of pure energy E, appears due to non-parabolicity of the band structure, γ' is its energy derivative, and E_g is the band gap. The scattering exponents take the values: $\lambda = -1/2$ for acoustic phonon scattering, $\lambda = 0$ for neutral impurity scattering, $\lambda = 1/2$ for polar optical phonon scattering, and $\lambda = 3/2$ for ionized impurity scattering.

Comparing the thermopower data in Fig. 2a to those reported in binary PbSe doped with Na, In, or Al,[37,40,41] shows that doubly-doped Eu + Na samples have considerably larger thermopower at given carrier concentration. Looking at the complete dataset in Fig. 2a and comparing to the theoretical curves, ionized impurity scattering likely is the reason for the increase in α. The resulting values of the power factors ($PF = \alpha^2/\rho$) in the studied samples are between 2 and 4 $\mu W\ K^{-2}\ cm^{-1}$ at room temperature. This contrasts with the values between 7 and 15 ($\mu W\ K^{-2}\ cm^{-1}$) that are reported[40] for solely Na-doped PbSe at similar carrier concentrations, as presented in Fig. 2b. The reduction in carrier mobility more than compensates the impact the increase in thermopower might have on the thermoelectric performance of the system.

Previous studies have reported that Eu exists as Eu^{2+} in PbSe[16,18] by analyzing its transport and magnetic properties. As a consequence, replacing Pb^{2+} with Eu^{2+} does not lead to any considerable changes in the carrier concentration (see, *e.g.* ref. 18). The Hall carrier concentration of the undoped $Pb_{0.99}Eu_{0.01}Se$ sample in our studies ($3 \times 10^{18}\ cm^{-3}$) is an order of magnitude lower than one would calculate if Eu was considered an electrically active element, confirming the previous results, and results from a small number of Pb vacancies. In the next section, the magnetic properties confirm that Eu is present as Eu^{2+} in PbSe without Na-doping. This behavior changes when the PbEuSe system is doped with Na, as can be seen in Fig. 1 and 2. First, substitution of Pb with Eu in $Pb_{1-y}Na_ySe$ greatly reduces the carrier concentration at the same Na concentration. The sample with ($x = 0$, $y = 0.01$), *i.e.* doped with 1% Na only, shows highly-degenerate semiconducting properties with approximately $2.1 \times 10^{20}\ cm^{-3}$ hole concentration at $T = 80$ K. This is close to the nominal carrier concentration of $1.75 \times 10^{20}\ cm^{-3}$, calculated if each monovalent Na^+ would give a single hole to the system. After introducing 1 at% of Eu ($x = 0.01$, $y = 0.01$), the hole concentration of the sample drops to about $6.0 \times 10^{19} cm^{-3}$. This effect cannot be explained if Eu was still Eu^{2+} as in $Pb_{1-x}Eu_xSe$, since in such a case, isovalent doping should have minimal impact on the carrier concentration. Moreover, continuous reduction in carrier concentration with higher Eu levels in ($y = 0.01$; $x > 0.01$) samples is observed, although to a lesser degree, and we reach $p \sim 2$–$3 \times 10^{19}\ cm^{-3}$ ($T = 80$ K) for ($x = 0.03 - 0.06$, $y = 0.01$).

The proposed explanation of the order-of-magnitude reduction in the carrier concentration of $Pb_{0.99-x}Eu_xNa_{0.01}Se$ is a change of the valence of a fraction of the Eu ions from Eu^{2+} to Eu^{3+}, where Eu^{3+} acts as an one-electron donor compensating the acceptor behavior of Na^+. Since electronic configuration of neutral Eu is $[Xe]4f^76s^2$, Eu^{2+} has seven 4f electrons, which are not mobile. Now, the release of one electron changes Eu^{2+} to Eu^{3+}, resulting in a $4f^6$ configuration of the Eu^{3+} ion with 3 mobile, valence electrons. Eu^{3+} now has one hole in the 4f shell. However, this 4f-like hole, as typical for all f-like states, is localized; thus, it does not take part in transport phenomena and cannot be detected by the Hall effect measurements. As the final effect, the presence of trivalent Eu^{3+} partly compensates the p-type doping efficiency of monovalent Na^+, when both are substituting for divalent Pb^{2+}. The effectiveness of this compensation and the ratio of the number of Eu^{2+}–Eu^{3+} ions can be estimated simply by comparing the measured carrier concentrations. For the Eu-free case, $Pb_{0.99}Na_{0.01}Se$, the measured hole concentration is about $2.1 \times 10^{20}\ cm^{-3}$, and it drops to

6.0×10^{19} cm^{-3} in $Pb_{0.98}Eu_{0.01}Na_{0.01}Se$. Now, assuming that all the difference comes from compensation of holes by electrons delivered while forming Eu^{3+}, the concentration of these electrons is 21×10^{19} cm^{-3}–6.0×10^{19} cm^{-3} = 15×10^{19} cm^{-3}, which means that 86% of the total number of Eu ions become Eu^{3+}. Thus, addition of 1 at% of Eu to the $Pb_{0.99}Na_{0.01}Se$ sample compensates about 86% of the holes delivered by 1 at% of Na atoms, and results in the Eu^{2+} : Eu^{3+} ratio of 14 : 86. When the Eu concentration increases, the amount of europium atoms in the Eu^{3+} donor state increases, further reducing the hole concentration in the samples. The results of the analysis performed for other samples are collected in Table 1, and, *e.g.*, for the $x = 0.02$, $y = 0.01$ case, about 45% of Eu has to be transformed into Eu^{3+} to explain the low carrier concentration of the sample, leaving only 55% Eu as Eu^{2+}.[42] In addition to the analysis of the carrier concentration in a set of $Pb_{0.99-x}Eu_xNa_{0.01}Se$ samples, the room temperature carrier concentration in a second set of samples, $Pb_{0.99-y}Eu_{0.01}Na_ySe$, was measured, where Eu concentration was kept at 1% and Na concentration was increased between 1% and 4%. According to Table 1, the carrier concentrations of ($x = 0$, $y = 1$) and ($x = 1$, $y = 2$) are very much similar (1.9×10^{20} and 1.7×10^{20} at 300 K, respectively). This also supports the idea of charge transfer between Na^+ and Eu^{2+}. 1 at% of Na^+ in the sample of ($x = 1$, $y = 2$) takes additional electrons and transforms Eu^{2+} to Eu^{3+}. Hence, only the other 1 at% of Na acts as the p-type doping agent in the sample, showing a carrier concentration that is close to that of ($x = 0$, $y = 1$). For the larger Na concentrations, most of Eu is at the Eu^{3+} configuration. This confirms that increasing the Na concentration triggers the transition from Eu^{2+} to Eu^{3+}.

The Pisarenko plot in Fig. 2 is consistent with this hypothesis. As mentioned above, the PbEuSe:Na data points align well with the "ionized scattering" $\alpha(p)$ curve, whereas the PbSe:Na points are below, near the polar optical phonon or neutral impurity scattering curves. That means that Eu^{3+}, not Na^+, is the source of the additional scattering. This also agrees with the presence of part of Eu in the 3+ state, ionized with respect to Pb^{2+}, but the scattering may be enhanced generally by the presence of Eu 4f electrons.

B. Magnetization of $Pb_{1-x-y}Eu_xNa_ySe$

As the two Eu ions, Eu^{2+} and Eu^{3+}, have different magnetic properties, magnetization measurements were carried out to verify the hypothesis further. According to Hund's rule, the total angular quantum number ($S_0 = |L - S|$) of Eu^{2+} is 7/2 (total orbital angular momentum $L = 0$, and spin $S = 7/2$), which gives the 7 μ_B magnetic moment of Eu^{2+}. On the other hand, theoretical S_0 of Eu^{3+} is zero ($L = 3$ and $S = 3$ cancel each other), giving zero magnetic moment of Eu^{3+}. Experimentally,[43] small magnetic moments were reported for Eu^{3+}, but the key is that any existence of Eu^{3+} instead of Eu^{2+} always results in a significant reduction in magnetization of the system. No change in magnetization is expected with Na addition if the Eu remains in the valence state 2+. Thus, magnetization measurements are a very sensitive tool to confirm or exclude the hypothesis of Eu^{2+}–Eu^{3+} transition in our samples.

The measured magnetization curves of ($y = 0.01$; $x = 0.01$, 0.02, 0.03, 0.06, 0.09, and 0.12) and ($x = 0.01$; $y = 0$, 0.01, 0.02, 0.03, and 0.04) as a function of magnetic field at 2 K are displayed in Fig. 3a and b, respectively. The weak diamagnetic contribution of PbSe matrix, with susceptibility $\chi_d = -3.6 \times 10^{-7}$ emu (g Oe)$^{-1}$ was subtracted, assuming that it is temperature independent. First, in samples with fixed Na concentration ($y = 0.01$; $x \geq 0.01$), the magnetization increases with Eu content x (Fig. 3a). This verifies that Eu gets incorporated into each sample proportionally to the amount of Eu added. In contrast to this expected behavior, the evolution of magnetic properties of $Pb_{1-x-y}Eu_xNa_ySe$ with y shows anomalous reduction of magnetic signal, that confirm the Eu^{2+}–Eu^{3+} transition in the system independently from the anomalies in the Hall coefficient, as explained below.

The following analysis of magnetic data starts from the magnetization of the 1 at% Eu doped, Na-free sample ($x = 0.01$, $y = 0$, black top curve in Fig. 3b). $M(B)$ at 2 K shows typical paramagnetic, Brillouin-like function shape, and the saturation magnetization value corresponds to the expected value for Eu^{2+} ion (7 μ_B, *i.e.* 1.27 emu g^{-1}) if the actual concentration of Eu atoms in the sample is 0.93% instead of 1%. Such a small discrepancy is consistent with a small loss of Eu during the synthesis. Thus, in agreement with previous reports[16,18] and the small carrier

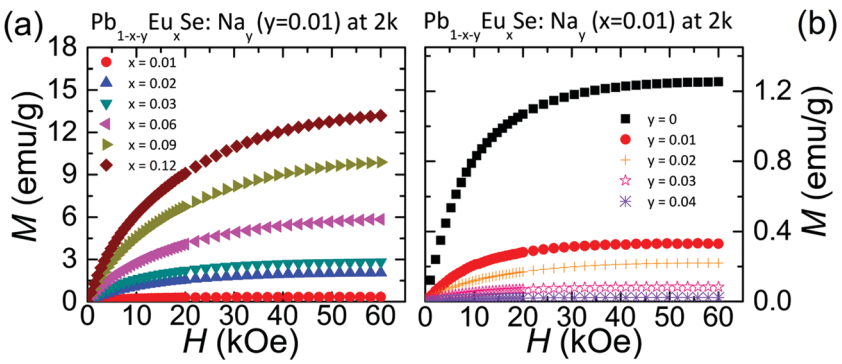

Fig. 3 (a) Magnetization of $Pb_{1-x-y}Eu_xNa_ySe$ ($y = 0.01$) with varying Eu level (x) as a function of magnetic field; (b) magnetization of $Pb_{1-x-y}Eu_xNa_ySe$ ($x = 0.01$) with varying Na doping level (y) as a function of magnetic field.

concentration measured in this sample, we observe that the Eu valence is 2+ in the absence of Na in PbSe.

When 1 at% of Na is added to $Pb_{0.99}Eu_{0.01}Se$, the magnetization of the sample drops more than three times, which is an independent signature of the transition of the majority of magnetic Eu^{2+} ions into non-magnetic Eu^{3+}. Fig. 3b shows how the magnetization decreases further with increasing Na doping levels, with the sample with 4 at% Na and 1 at% Eu reaching a saturation magnetization of less than 2% of that of undoped $Pb_{0.99}Eu_{0.01}Se$. Here, almost all of the Eu ions are transformed into Eu^{3+}. This observation is consistent quantitatively with the reduction observed for the carrier concentration (Fig. 1a), where adding Eu compensated the donor behavior of Na. The actual amount of Eu^{2+} in each sample, denoted here as $x_{Eu^{2+}}$, deduced based on the saturation of experimental magnetization data and assuming 7 μ_B magnetic moment of Eu^{2+} ions, is presented in Table 1. The mixed-valence behavior, where part of the Eu is in the 2+ and the rest is in the 3+ state, is especially visible for the samples with 1 at% Na and 3–6 at% of Eu. It is worth noting, that Eu^{2+} concentrations deduced from magnetization are close to those obtained from the carrier concentration analysis. However, the Eu^{2+} concentrations deduced from magnetization measurements should be considered as more accurate, since the accuracy of Hall carrier concentration is limited by the accuracy of the formula ($p = -1/eR_H$, e – electron charge), and can be affected by Hall prefactors that depend on the scattering mechanism. This is the most likely reason for the differences between the two columns in Table 1.

The low-temperature field dependence of the magnetization deviates slightly but measurably from the Brillouin function that characterizes the magnetic moment of pure paramagnets. The magnetization data of the samples with ($x = 0.01$, $y = 0$) and ($x = 0.03$, $y = 0.01$) at $T = 2$ K, 4 K and 6 K, as a function of magnetic field, are reported in Fig. 4. The field and temperature dependence of the magnetization of the independent non-interacting (paramagnetic) Eu^{2+} ions M_{BR} is described by:[43,44]

$$M_{BR} = M_0 S_0 x_{Eu^{2+}} B_{S_0}(\xi) \quad (2)$$

where B_{S_0} is the Brillouin function, $B_{S_0}(\xi) = \frac{2S_0+1}{2S_0}\coth\frac{2S_0+1}{2S_0}(\xi) - \frac{1}{2S_0}\coth\frac{1}{2S_0}(\xi)$, $\xi = \frac{g\mu_B S_0 H}{k_B T}$, $S_0 = 7/2$, $M_0 = g\mu_B N_A/m(x_{Eu^{2+}})$, $m(x_{Eu^{2+}})$ is the molar mass of the compound, g is the g-factor of Eu^{2+} (we take $g = 2$), N_A is Avogadro's number, and μ_B is the Bohr magneton. Fig. 4a and c represent the field-dependent magnetization data fitted to M_{BR} (solid lines) at each temperature. At low field, the sample with ($x = 0.01$, $y = 0$) has slightly lower magnetization data when fitted to M_{BR}, suggesting the presence of antiferromagnetic (AF) interactions between Eu ions in the sample, as reported in earlier works for Eu-doped PbSe.[16] The increase in Eu level in PbSe results in a larger deviation from M_{BR} as seen in Fig. 4c for ($x = 0.03$, $y = 0$) sample. However, with the increase in temperature, AF interactions are overcome by thermal excitations, giving better fitting of the data to M_{BR}; the data obtained at $T = 6$ K fits M_{BR} reasonably well.

To analyze the strength of AF interactions, a model, denoted here as M_{AF_BR}[16,44,45] is used. The model takes into account antiferromagnetic interactions between the nearest neighbor (NN) Eu ions. If random arrangement of magnetic ions in the

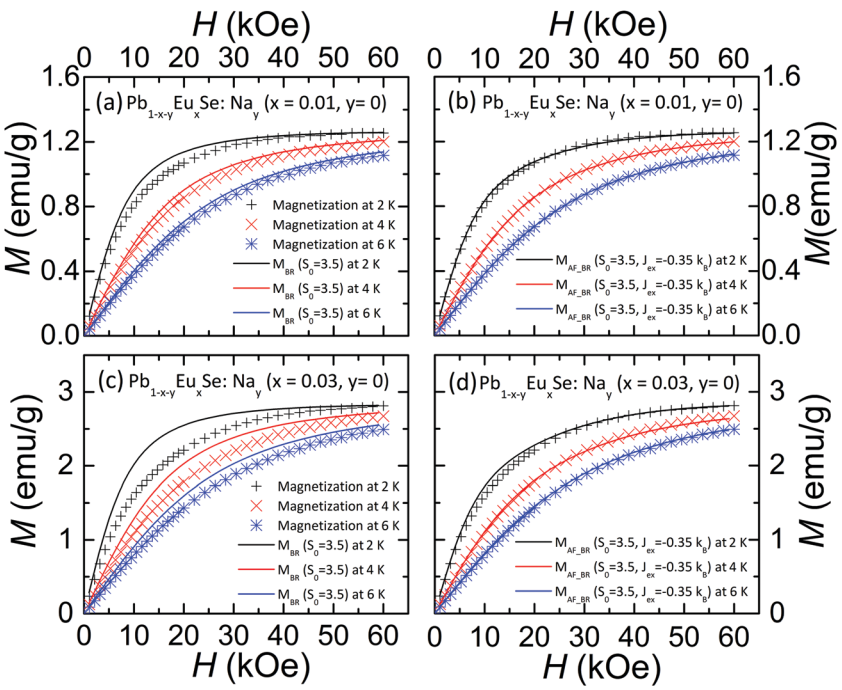

Fig. 4 Magnetization of two $Pb_{1-x-y}Eu_xNa_ySe$ samples as a function of magnetic field. Solid lines in panels (a) and (c) are the curves of the calculated magnetization with Brillouin function (without corrections for the AF interaction). Solid lines in panels (b) and (d) are model (M_{AF_BR}) curves that consider AF contributions of pairs and triplets to the magnetization. The much better agreement between the measured data and models on panels (b) and (d) *versus* (a) and (c) is clearly visible.

crystal lattice is assumed, up to several percent Eu concentration, we have a noticeable probability of finding Eu not only in an isolated, single configuration (*i.e.* no other Eu as NN), but also in pairs (two Eu as NN) and triplets (three Eu as NN). For the last case we have two possibilities, open triplets (first and third Eu are not NN, like in a chain) and closed triplets (equilateral triangle, *i.e.* all Eu are NN). Higher order combinations can be neglected up to about 3–4% of magnetic ions[46]. In this way, the total magnetization (M_{AF_BR}) can be described as $M_{AF\_BR} = M_S + M_P + M_{OT} + M_{CT}$, where M_S, M_P, M_{OT}, and M_{CT} are the contributions to magnetization from singles, pairs, open triplets, and closed triplets, respectively. The singles' contribution (M_S) in a model (M_{AF_BR}) is the same as eqn (2), but the probability P_S of finding the singles in the sample is taken into account. Hence, the single contribution (M_S) is

$$M_S = M_{BR}P_S. \quad (3)$$

The pair contribution (M_P) is[16,44,45]

$$M_P = \frac{1}{2}M_0 P_P x_{Eu^{2+}} \times \frac{\sum_{S=0}^{S=S_{MAX}} \exp\left(\frac{J_{ex}}{k_B T}S(S+1)\right) S\left(\sinh\left(\frac{2S+1}{2S}\xi\right)\right) B_J(\xi)}{\sum_{S=0}^{S=S_{MAX}} \exp\left(\frac{J_{ex}}{k_B T}S(S+1)\right)\left(\sinh\left(\frac{2S+1}{2S}\xi\right)\right)} \quad (4)$$

where $S_{MAX} = 2S_0$, J_{ex} is the exchange coupling parameter, and k_B is the Boltzmann constant.

The open triplet contribution (M_{OT}) and the closed triplet contribution (M_{CT}) are listed below:

$$M_{OT} = \frac{1}{3}M_0 P_{OT} x_{Eu^{2+}} \frac{\sum_{S_a}\sum_{S_b}\sum_{m} m \exp\left(-E_{OT}(S_a, S_b, m)\frac{1}{k_B T}\right)}{\sum_{S_a}\sum_{S_b}\sum_{m} \exp\left(-E_{OT}(S_a, S_b, m)\frac{1}{k_B T}\right)} \quad (5)$$

$$M_{CT} = \frac{1}{3}M_0 P_{CT} x_{Eu^{2+}} \frac{\sum_{S_a}\sum_{S_b}\sum_{m} m \exp\left(-E_{CT}(S_a, S_b, m)\frac{1}{k_B T}\right)}{\sum_{S_a}\sum_{S_b}\sum_{m} \exp\left(-E_{CT}(S_a, S_b, m)\frac{1}{k_B T}\right)} \quad (6)$$

where $E_{OT} = -mg\mu_B H - J_{ex}(S_b(S_b + 1) - S_a(S_a + 1) - S_0(S_0 + 1)$, $E_{CT} = -mg\mu_B H - J_{ex}(S_b(S_b + 1) + 3S_0(S_0 + 1)))$, and $0 \le S_a \le 7, \left|S_a - \frac{7}{2}\right| \le S_b \le S_a + \frac{7}{2}$, and $|m| \le S_b$.

The probabilities of finding the singles (P_S), the pairs (P_P), and the triplets (P_{OT} and P_{CT}) of Eu ions in the rock salt fcc lattice are shown below:[46]

$$P_S = (1 - x_{Eu^{2+}})^{12}$$
$$P_P = 12x_{Eu^{2+}}(1 - x_{Eu^{2+}})^{18} \quad (7)$$
$$P_{OT} = 18x_{Eu^{2+}}{}^2(1 - x_{Eu^{2+}})^{23}(5(1 - x_{Eu^{2+}}) + 2)$$
$$P_{CT} = 24x_{Eu^{2+}}{}^2(1 - x_{Eu^{2+}})^{22}$$

These probabilities are valid under the assumption of completely random distribution of Eu ions in the samples.

The formulas above are used to fit the magnetization data in Fig. 4b and d. Note, that the procedure involves only two fitting parameters: $x_{Eu^{2+}}$, fitting the saturated part of the magnetization, and the exchange interaction parameter, J_{ex}, describing the antiferromagnetic contribution to magnetization, seen for lower fields (J_{ex} was kept constant for all analyzed curves). When AF interactions between Eu ions (singles, pairs, and triplets) are considered, the best fitting curve is found with $J_{ex}/k_B = -0.35$ K; nearly all the magnetization data lies on the curve as shown in Fig. 4b and d, considerably improving the fitting against the Fig. 4a and c. This supports the notion that the exchange interaction between nearest neighbor of Eu^{2+} ions in PbSe is antiferromagnetic.

A previous study[16] has also reported AF interactions of Eu^{2+} ions in $Pb_{1-x}Eu_xSe$ samples with $J_{ex}/k_B = -0.24$ K at $T = 0.62$ K from the magnetization steps analysis, whereas our obtained exchange coupling (J_{ex}/k_B) is slightly different, $J_{ex}/k_B = -0.35$ K from $T = 2$ K to 6 K. The difference may come from the different carrier concentration of the samples; however, further studies at lower temperatures would be necessary to conclude this. It should be mentioned that an increase in the Eu concentration in PbSe will also increase the probability of forming structures of NN Eu atoms that are larger than simple triangles in which the AF interactions play a role. For this reason, the magnetization fittings in the samples with ($x > 0.03$, $y = 0.01$) are not reported. For example, the total probability of the analyzed configuration, $P_T = P_S + P_P + P_{OT} + P_{CT}$ of ($x = 0.03$, $y = 0.01$) sample is 99%, while that of ($x = 0.06$, $y = 0.01$) sample would be 92%, hence 8% of the total magnetization is delivered by the higher-order configurations (squares, *etc.*), and the analysis limited to triangles becomes not accurate enough and is not presented.

In Fig. 5, the inverse low field (5 kOe) susceptibility against temperature in three samples of $Pb_{1-x-y}Eu_xSe{:}Na_y$ with ($x = 0.01$, $y = 0$) ($x = 0.03$, $y = 0.01$), and ($x = 0.06$, $y = 0.01$) is reported. The data are analyzed using the Curie–Weiss law:[43]

$$\chi = \frac{C}{T + \theta} + \chi_d \quad (8)$$

where T is the absolute temperature, χ_d is the diamagnetic susceptibility, C is the Curie constant, and θ is the Curie–Weiss temperature as given by[47]

$$C = \frac{x_{Eu^{2+}} N g^2 \mu_B{}^2 S_0(S_0 + 1)}{3k_B} \quad (9)$$

$$\theta = \frac{2x_{Eu^{2+}} S_0(S_0 + 1)}{3k_B} z J_{ex} \quad (10)$$

In (9) and (10), N is $\frac{N_A}{m(x_{Eu^{2+}})}$, $\mathbf{z}$ is the number of sites on the coordination sphere ($z = 12$), and J_{ex}/k_B is the exchange constant. Using the same $J_{ex}/k_B = -0.35$ K and number of magnetic Eu^{2+} ions $x_{Eu^{2+}}$ as is the low-temperature magnetization analysis (Table 1), we are able to describe the susceptibility behavior,

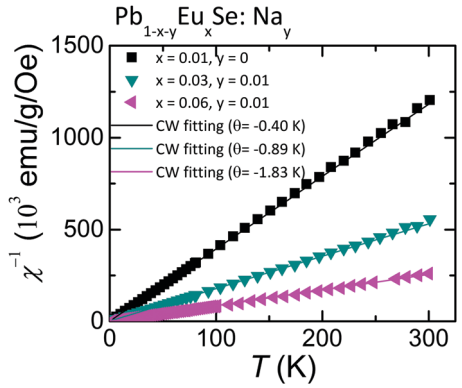

Fig. 5 Inverse susceptibility of three $Pb_{1-x-y}Eu_xNa_ySe$ samples as a function of temperature. The solid lines are obtained from the Curie–Weiss law, eqn (8).

as seen in Fig. 5, where the low field magnetic (5 kOe) susceptibility data shows linear relation with temperature, following the Curie–Weiss law. This supports the conclusion of the presence of AF interactions between nearest neighboring Eu atoms (negative θ and J_{ex}), as well as the transformation of Eu^{2+} to Eu^{3+} with Na doping (the same $x_{Eu^{2+}}$ used here).

C. Electronic structure

The experimental data analysis provides strong evidence that the Eu valence in $Pb_{1-x-y}Eu_xNa_ySe$ varies from 2+ to 3+. The question that remains open at this point is whether this transition may be explained by the evolution of the electronic band structure of the system, or whether it is connected to the chemistry of the material (*e.g.*, formation of an antiferromagnetic Eu–Se secondary phases could also decrease the total magnetization of the samples, although it would not be consistent with the close correlation of the drop in magnetization with the carrier concentration change). The electronic structure calculations in this section address the question. This is a difficult task for density functional (DFT) methods, since the presence of a 4f element (Eu) requires taking into account strong Coulomb interactions on the 4f shell. Furthermore, the system under study is double-doped (Eu + Na). The Eu^{2+}–Eu^{3+} transition, proposed here to explain the behavior of the Hall charge density and magnetization, would be consistent with the presence of the highest occupied Eu 4f level near the Fermi energy E_F of PbSe, so that changes in E_F with Na doping can move the Fermi energy into the Eu 4f level, leading to an instability of the $4f^7$ configuration and driving the transition to the mixed $4f^6$–$4f^7$ state.

The calculated densities of states (DOS) for three concentrations of Eu and Na in PbSe are presented in Fig. 6. First, in panel (a), DOS of 64-atom PbSe supercell with a single Pb replaced with Eu (*i.e.* $Eu_1Pb_{31}Se_{32}$) is shown. This corresponds to about 3 at% of Eu in PbSe. We see full spin-polarization of the Eu 4f states, with the empty spin-down states expelled well above E_F (not shown for clarity of the figure). A semiconducting state is seen in panel (a), with Eu $4f^7$ occupied configuration and spin magnetic moment of 7 μ_B per Eu, confirming the Eu^{2+} state in PbSe. The first peak of the Eu $4f^7$ shell DOS is about 0.25 eV below the valence band edge. Panels (b) and (c) in Fig. 6 show two cases of doubly doped PbSe, $Eu_1Na_3Pb_{28}Se_{32}$ in panel (b) and $Eu_2Na_2Pb_{28}Se_{32}$ in panel (c). In these supercells, the symmetry was reduced to trigonal, to allow for different configurations of Eu and Na atoms within the same computational geometry. When Na is introduced into $Pb_{1-x}Eu_xSe$ (see, Fig. 6b), the Fermi level moves deep into the valence band (VB), and the 4f Eu shell DOS splits into two main parts. One, accommodating six 4f electrons, goes deeper into the VB, corresponding to a stable $4f^6$ configuration. The second, accommodating single electron, remains near the VB edge, with E_F inside the peak. The total filling of the 4f shell here is 6.7. Such a configuration, with E_F being inside the 4f peak with a large spectral weight of f-states at the Fermi level and a partial 4f shell filling, cannot be stable in the real material and should be interpreted as an "averaged" picture of the mixed $4f^6$–$4f^7$ state, predicted by the static, single-electron density functional computations. The $Eu^{2+}(4f^7)$–$Eu^{3+}(4f^6)$ transition avoids such energetically unfavorable electronic configuration, and the real DOS in the material will not look like the one presented in Fig. 6b, which should be treated as a signature of the valence

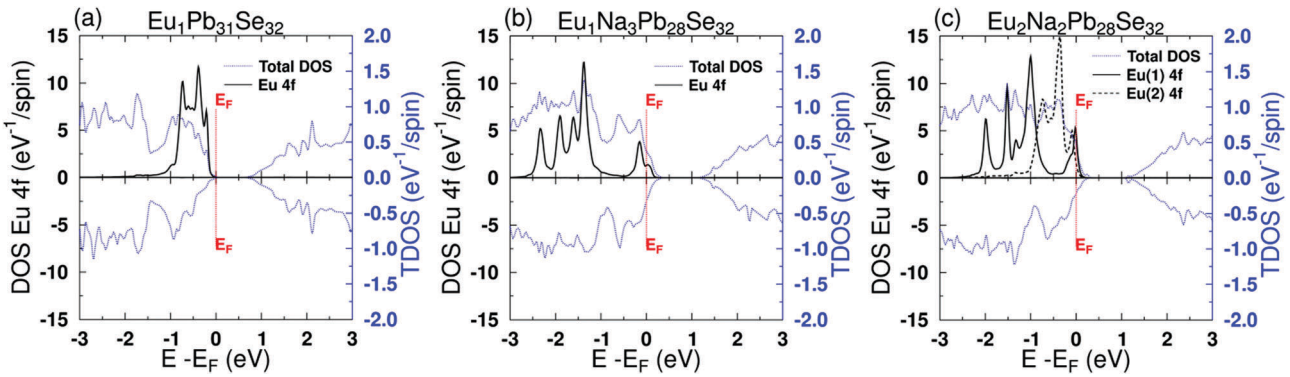

Fig. 6 Spin-polarized densities of states (DOS) for 64-atoms supercells of PbSe, with some of Pb atoms substituted by Eu and Na, as given in the top legend. On each of the panels, the "spin-down" DOS is plotted as negative. The left scale corresponds to the partial 4f Eu DOS (black curves) given per Eu atom and per spin, while the right scale gives the total DOS of the supercell (blue curves), divided by 32 (the number of PbSe formula units).

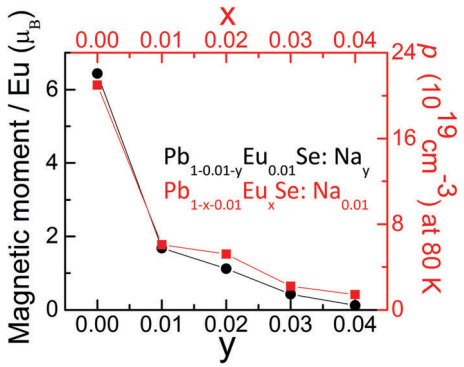

Fig. 7 Correlation between the measured magnetic moment per Eu atom, obtained from the fitting of $Pb_{1-x-y}Eu_xNa_ySe$ (x = 0.01; y = 0, 0.01, 0.02, 0.03, and 0.04) magnetization data (left scale, black points), and the carrier concentration at T = 80 K (y = 0, 0.01; x = 0.01, 0.02, 0.03, and 0.04) (right scale, red squares).

instability. Similar results (Fig. 6c) were obtained for the third studied supercell, $Eu_2Na_2Pb_{28}Se_{32}$, in which the two Eu atoms were located in two inequivalent crystallographic positions with different Eu–Na distance. Also here, as the Fermi energy comes close to the Eu-4f DOS, the reconfiguration of the Eu 4f shell takes place. The Eu(1) atom, located closer to Na, exhibits larger splitting of the 4f shell and stronger reduction of the $4f^7$-th level filling (equal to 6.6), comparing to Eu(2) (filling equal to 6.8), which was placed much further from Na [the distances were: Eu(1)–Na 4.3 Å, Eu(2)–Na 7.5 Å]. This is understood, as the smaller valence electron density around Na^+, compared to Pb^{2+}, lies behind the Eu^{2+}–Eu^{3+} transition, so the Eu(1) ion located closer to Na^+, should adopt the $4f^6$ configuration more readily than Eu(2). On the other hand, this also shows that no Eu–Na clustering effects are necessary to trigger the Eu^{2+}–Eu^{3+} transition; for the Eu(2) atom, the nearest Na was located as far as the 6th coordination sphere.

Note that presented results cannot determine whether the valence "mixing" is in the time domain (valence fluctuations) or in the space domain (static spatially mixed valence). Also, the calculated fraction of Eu^{3+} is a slower function of the Na concentration than that observed in the real material. The magnetization data (Table 1) show that in the samples with 1% Eu and 1% Na concentrations, 76% of Eu is in the 3+ state. In contrast, from DFT studies in $Eu_2Na_2Pb_{28}Se_{32}$ one sees that the average Eu 4f shell filling is 6.7, which could be interpreted as 30% of Eu in Eu^{3+} state. Nevertheless, DFT computations gave theoretical and independent support to the hypothesis of a Eu^{2+}–Eu^{3+} valence transition in the studied system. Moreover, a qualitative explanation of the mechanism of transition is given, in terms of the modifications in the electronic structure of the system triggered by the unfavorable location of the Fermi energy inside the DOS of the Eu-4f electron shell.

Summary and conclusion

We have investigated thermoelectric, galvanomagnetic, magnetic, and electronic properties of $Pb_{1-x-y}Eu_xSe{:}Na_y$ samples. The measurement results are summarized in Fig. 7, which represents magnetization and hole concentration as a function of both Eu and Na content.

First, as the Eu level (x) in $Pb_{0.99-x}Eu_xNa_{0.01}Se$ is increased, the system shows a significant reduction in hole concentration. Second, when Na level (y) is increased in $Pb_{0.99-y}Eu_{0.01}Na_ySe$, an equally significant decrease in magnetization is observed. Both phenomena can be explained by the valence transition of a fraction of the europium atoms, from magnetic and divalent Eu^{2+} to a non-magnetic and trivalent Eu^{3+}, when Na is added to the system and the position of the Fermi level changes. As a result, a mixed valence state is realized in the system, and each amount of Eu in a 3+ state compensates a fraction of holes delivered by Na. When the concentrations of Eu and Na are both equal to 1%, 76% of Eu^{2+} ions are transformed into Eu^{3+}. When the concentration of Na is further increased, the percentage of trivalent Eu is rising, reaching 98% for x = 1%, y = 4% case. A simplified electron-counting model for this transition would be that the Eu^{2+} concentration would change with the introduction of Na^+, into Eu^{3+} and Na^0. Fig. 7 then illustrates how any loss of Na^+ causes an increase in the amount of non-magnetic Eu^{3+} and a decrease in carrier concentration. Electronic structure calculations showed that the highest energy Eu 4f level of the Eu^{2+} ion in PbSe is located about 0.25 eV below the VB edge of the system. When Na, which is an acceptor in PbSe, is added to $Pb_{1-x}Eu_xSe$, E_F moves deeper into the VB, causing an instability and splitting of the Eu-4f electronic shell. This independently supports the idea of Eu^{2+}–Eu^{3+} valence transition in the double-doped $Pb_{1-x-y}Eu_x\ Na_ySe$.

Moreover, we observed and analyzed magnetic interactions between the Eu ions in the studied samples. Low-temperature magnetization data are fitted successfully to a model that takes into account the magnetic contributions of singles, pairs, and triplets of Eu^{2+} ions. Antiferromagnetic interaction between the nearest-neighbor Eu^{2+} with exchange coupling of $J_{ex}/k_B = -0.35$ K was found. This was confirmed further by the low-field susceptibility measurements, analyzed using the Curie–Weiss law and taking the same exchange constant.

The important question that remains open and should be addressed in future studies, is whether the Eu^{2+}–Eu^{3+} transition will take place for acceptors other than Na in $Pb_{1-x}Eu_xSe$. If the interpretation presented here is correct, the answer should be positive, since the interpretation does not involve the chemical nature of Na, but is based on a shift of the Fermi levels and a reconfiguration in $Pb_{1-x}Eu_xSe$ bands. In other words, the rigid band approximation applies to additions of Na, but not to additions of Eu, even if the amounts added are similar. Furthermore, a similar behavior may be possible in other rare-earth doped narrow-gap semiconductors and hints of a behavior similar to that described here might have been seen in InSb doped with Er[48] and Sm[49].

Acknowledgements

This work is supported as part of the Center for Revolutionary Materials for Solid State Energy Conversion, an EFRC funded by

the U.S. DOE, Office of Science, Office of Basic Energy Sciences under Award Number DE-SC0001054. JPH is partly supported by the ARO MURI "Materials with extraordinary spin-heat coupling" under grant W911NF-14-1-0016. BH is supported by the NSF EFRI-2DARE grant number 1433467. BW was partly supported by the Polish National Science Center (project no. DEC-2011/02/A/ST3/00124).

Notes and references

1 A. F. Ioffe, *Semiconductor Thermoelements and Thermoelectric Cooling*, Infosearch, London, 1957.
2 K. Yang, W. Setyawan, S. Wang, M. Buongiorno Nardelli and S. Curtarolo, *Nat. Mater.*, 2012, **11**, 614.
3 J. P. Heremans, V. Jovovic, E. S. Toberer, A. Saramat, K. Kurosaki, A. Charoenphakdee, S. Yamanaka and G. J. Snyder, *Science*, 2008, **321**, 554.
4 K. F. Hsu, S. Loo, F. Guo, W. Chen, J. S. Dyck, C. Uher, T. Hogan, E. K. Polychroniadis and M. G. Kanatzidis, *Science*, 2004, **303**, 818.
5 P. F. P. Poudeu, J. D'Angelo, A. D. Downey, J. L. Short, T. P. Hogan and M. G. Kanatzidis, *Angew. Chem., Int. Ed.*, 2006, **45**, 3835.
6 K. Biswas, J. He, I. D. Blum, C.-I. Wu, T. P. Hogan, D. N. Seidman, V. P. Dravid and M. G. Kanatzidis, *Nature*, 2012, **489**, 414.
7 Y. Lee, S.-H. Lo, J. Androulakis, C.-I. Wu, L.-D. Zhao, D.-Y. Chung, T. P. Hogan, V. P. Dravid and M. G. Kanatzidis, *J. Am. Chem. Soc.*, 2013, **135**, 5152.
8 J. Androulakis, Y. Lee, I. Todorov, D.-Y. Chung and M. G. Kanatzidis, *Phys. Rev. B: Condens. Matter Mater. Phys.*, 2011, **83**, 195209.
9 G. Bauer, H. Pascher and W. Zawadzki, *Semicond. Sci. Technol.*, 1992, **7**, 703.
10 H. Kanazawa, S. Adachi, T. Yamaguchi, S. Murashige and K. Murakami, *J. Appl. Phys.*, 1999, **86**, 2611.
11 A. Lambrecht, N. Herres, B. Spanger, S. Kuhn, H. Bottner, M. Tacke and J. Evers, *J. Cryst. Growth*, 1991, **108**, 301.
12 G. Braunstein, G. Dresselhaus, J. Heremans and D. Partin, *Phys. Rev. B: Condens. Matter Mater. Phys.*, 1987, **35**, 1969.
13 J. Heremans and D. L. Partin, *Phys. Rev. B: Condens. Matter Mater. Phys.*, 1988, **37**, 6311.
14 D. L. Partin, J. Heremans, C. M. Thrush, L. Green and C. H. Olk, *Phys. Rev. B: Condens. Matter Mater. Phys.*, 1988, **38**, 3549.
15 L. Salamanca-Young, D. L. Partin and J. Heremans, *J. Appl. Phys.*, 1988, **63**, 1504.
16 V. Bindilatti, N. F. Oliveira, Jr., Y. Shapira, G. H. McCabe, M. T. Liu, S. Isber, S. Charar, M. Averous, E. J. McNiff, Jr. and Z. Golacki, *Phys. Rev. B: Condens. Matter Mater. Phys.*, 1996, **53**, 5472.
17 S. Isber, S. Charar, C. Fau, V. Mathet, M. Averous and Z. Golacki, *Phys. Rev. B: Condens. Matter Mater. Phys.*, 1995, **52**, 1678.
18 V. Jovovic, S. J. Thiagarajan, J. West, J. P. Heremans, T. Story, Z. Golacki, W. Paszkowicz and V. Osinniy, *J. Appl. Phys.*, 2007, **102**, 043707.
19 V. Zlatic and R. Monnier, *Modern Theory of Thermoelectricity*, Oxford University Press, 2015.
20 T. Story, Semimagnetic Semiconductors Based on Lead Chalcogenides, in *Lead Chalcogenides: Physics and Applications*, ed. D. Khokhlov, Taylor & Francis, New York, 2003.
21 A. Lenard, T. Dietl, M. Sawicki, W. Dobrowolski, K. Dybko, T. Skośkiewicz, W. Plesiewicz, S. Miotkowska, A. Witek and A. Mycielski, *J. Low Temp. Phys.*, 1990, **80**, 15.
22 U. Zeitler, A. Wittlin, J. C. Maan, W. Dobrowolski and A. Mycielski, *Phys. Rev. B: Condens. Matter Mater. Phys.*, 1996, **54**, 15258.
23 W. Dobrowolski, *Acta Phys. Pol., A*, 1996, **89**, 3.
24 M. von Ortenberg, *Semicond. Sci. Technol.*, 1993, **8**, S16.
25 T. Dietl, *J. Cryst. Growth*, 1990, **101**, 808.
26 J. Mycielski, *Solid State Commun.*, 1986, **60**, 165.
27 E. Grodzicka, W. Dobrowolski, J. Kossut, T. Story and B. Witkowska, *Acta Phys. Pol., A*, 1993, **84**, 599.
28 T. Story, Ż. Wilamowski, E. Grodzicka, W. Dobrowolski, B. Witkowska and J. Voiron, *Acta Phys. Pol., A*, 1995, **87**, 229.
29 T. Story, M. Górska, A. Łusakowski, M. Arciszewska, W. Dobrowolski, E. Grodzicka, Z. Gołacki and R. R. Gałązka, New Mechanism of f- f Exchange Interactions Controlled by Fermi Level Position, *Phys. Rev. Lett.*, 1996, **77**, 3447.
30 T. Story, *Acta Phys. Pol., A*, 1996, **91**, 173.
31 E. Grodzicka, W. Dobrowolski, T. Story, E. I. Slynko, Yu.K. Vygranenko, M. M. H. Willekens, H. J. M. Swagten and W. J. M. de Jonge, *Acta Phys. Pol., A*, 1996, **90**, 801.
32 P. Blaha, K. Schwarz, G. K. H. Madsen, D. Kvasnicka and J. Luitz, *WIEN2K, An Augmented Plane Wave + Local Orbitals Program for Calculating Crystal Properties*, Karlheinz Schwarz, Technische Universität Wien, 2001.
33 J. Kuneš and R. Laskowski, *Phys. Rev. B: Condens. Matter Mater. Phys.*, 2004, **70**, 174415.
34 A. Rubio-Ponce, A. Conde-Gallardo and D. Olguín, *Phys. Rev. B: Condens. Matter Mater. Phys.*, 2008, **78**, 035107.
35 F. Tran and P. Blaha, *Phys. Rev. Lett.*, 2009, **102**, 226401.
36 Y. I. Ravich, B. A. Efimova and I. A. Smirnov, *Semiconducting lead chalcogenides*, Plenum Press, New York, 1970.
37 E. G. Evola, M. D. Nielsen, C. M. Jaworski, H. Jin and J. P. Heremans, *J. Appl. Phys.*, 2014, **115**, 053704.
38 in *Non-Tetrahedrally Bonded Elements and Binary compounds I, Lead Selenide (PbSe) Debye temperature, density, melting temperature*, ed. O. Madelung, U. Rossler and M. Schulz, Springer, Berlin, 1998, vol. 41C.
39 E. Evola, *High Figure of Merit Lead Selenide Doped with Indium and Aluminum for Use in Thermoelectric Waste Heat Recovery Applications at Intermediate Temperatures*, Electronic thesis, Ohio State University, 2012. https://etd.ohiolink.edu/pg_10?0::NO:10:P10_ACCESSION_NUM:osu1338307382.
40 T. C. Chasapis, Y. Lee, E. Hatzikraniotis, K. M. Paraskevopoulos, H. Chi, C. Uher and M. G. Kanatzidis, *Phys. Rev. B: Condens. Matter Mater. Phys.*, 2015, **91**, 085207.
41 H. Wang, Y. Pei, A. D. LaLonde and G. J. Snyder, *Adv. Mater.*, 2011, **23**, 1366.
42 Note, that if as a reference value, the nominal carrier concentration is used (1.75×10^{20} cm^{-3}, assuming that

each Na delivers one hole to the system), instead of the measured Hall value of 2.1×10^{20} cm^{-3}, given Eu^{2+}/Eu^{3+} concentrations are changed in about 15%.

43 N. W. Ashcroft and N. D. Mermin, *Solid State Physics*, Holt, Rinehart, and Winston, New York, 1976, p. 656, and references therein.

44 X. Gratens, S. Charar, M. Averous, S. Isber, J. Deportes and Z. Golacki, *Phys. Rev. B: Condens. Matter Mater. Phys.*, 1997, **56**, 8199.

45 Y. Shapira and V. Bindilatti, *J. Appl. Phys.*, 2002, **92**, 4155.

46 M. M. Kreitman and D. L. Barnett, *J. Chem. Phys.*, 1965, **43**, 364.

47 A. Errebbahi, S. Charar, F. Terki, C. Fau, S. Isber, M. Tabbal, T. C. Christidis, D. Ravot, J. C. Tedenac and Z. Golacki, *J. Magn. Magn. Mater.*, 2002, **247**, 55.

48 J. P. Heremans, D. L. Partin, D. T. Morelli and C. M. Thrush, *J. Vac. Sci. Technol., B*, 1992, **10**, 659.

49 D. L. Partin, J. P. Heremans, C. M. Thrush and D. T. Morelli, *J. Vac. Sci. Technol., B*, 1992, **10**, 873.

